Applied Physics Letters

Experimental realization of a silicon spin field-effect transistor

Biqin Huang, Douwe J. Monsma, and Ian Appelbaum

Citation: Appl. Phys. Lett. **91**, 072501 (2007); doi: 10.1063/1.2770656
View online: http://dx.doi.org/10.1063/1.2770656
View Table of Contents: http://apl.aip.org/resource/1/APPLAB/v91/i7
Published by the American Institute of Physics.

Experimental realization of a silicon spin field-effect transistor

Biqin Huang[a)]
Electrical and Computer Engineering Department, University of Delaware, Newark, Delaware 19716

Douwe J. Monsma
Cambridge NanoTech, Inc., Cambridge, Massachusetts 02139

Ian Appelbaum
Electrical and Computer Engineering Department, University of Delaware, Newark, Delaware 19716

(Received 29 May 2007; accepted 20 July 2007; published online 13 August 2007)

A longitudinal electric field is used to control the transit time (through an undoped silicon vertical channel) of spin-polarized electrons precessing in a perpendicular magnetic field. Since an applied voltage determines the final spin direction at the spin detector and hence the output collector current, this comprises a spin field-effect transistor. An improved hot-electron spin injector providing ≈115% magnetocurrent, corresponding to at least ≈37% electron current spin polarization after transport through 10 μm undoped single-crystal silicon, is used for maximum current modulation. © *2007 American Institute of Physics*. [DOI: 10.1063/1.2770656]

The spin field effect transistor (spinFET) proposed by Datta and Das[1] has stimulated much research in spin precession-controlled electronic semiconductor devices.[2–5] Because silicon (Si) has a very long intrinsic electron spin lifetime[6,7] and is the cornerstone of modern semiconductor microelectronics, it could be the materials basis of a future semiconductor spintronics paradigm utilizing these types of devices. However, spintronics techniques which worked so well for other semiconductors, most notably GaAs (Refs. 8–13) are ineffective with silicon for both band structure and material growth reasons.[7]

To solve this problem, we have recently demonstrated spin transport in silicon using hot-electron transport through ferromagnetic (FM) metal thin films for all-electrical spin-polarized injection and detection.[14] Because the device design includes rectifying Schottky barriers on either side of the Si transport layer, an applied accelerating voltage induces little spurious current, allowing transit-time control of final spin direction at the spin detector during precession in a perpendicular magnetic field. Two of us have recently proposed to use this effect as the basis of a transit-time spinFET.[15]

To demonstrate the transit-time spinFET, the output collector current magnetocurrent change must be larger than any magnetically independent current rise induced by accelerating voltage increase. However, operation of previously demonstrated devices in this proposed mode is prevented by the low magnetocurrent signal of only ≈2%, and the presence of a small, but significant, rise in collector current with accelerating voltage.[14]

One possible reason for this low spin injection efficiency could be a "magnetically dead" silicide layer[16–19] formed between the silicon and ferromagnetic metals used for injector and detector in this device. As we have already demonstrated,[20] by relocating the injector ferromagnetic layer away from the silicon Schottky interface, the spin injection efficiency increased by over an order of magnitude. In this letter, we demonstrate even higher magnetocurrent in silicon spin transport devices with a further modified injector structure utilizing ballistic spin filtering[21–23] and a Cu interfacial interlayer to prevent silicide formation with the FM layer. We then use this device to realize the transit-time spinFET.

A schematic illustration for our improved device in side view is shown in Fig. 1(a), together with its associated band diagram in Fig. 1(b). The injector structure is 40 nm Al/Al_2O_3/5 nm Al/5 nm $Co_{84}Fe_{16}$/5 nm Cu. Unpolarized electrons tunneling from the normal metal Al across the Al_2O_3 oxide barrier are subsequently spin polarized by the hot-electron ballistic spin filtering effect (spin-dependent scattering) through the $Co_{84}Fe_{16}$ layer before conduction band injection over the Cu/Si Schottky barrier.

After vertical transport through the 10 μm thick undoped single-crystal silicon device layer, the spin-polarized electrons are ejected from the Si conduction band into the detector FM thin film ($Ni_{80}Fe_{20}$) above the Fermi energy. The ballistic component of this hot-electron current is collected by the second Schottky barrier with a *n*-Si substrate, forming the collector current and spin-transport signal (I_{C2}). By manipulating the relative orientation of the injector and detector FM layer magnetizations with an in-plane external magnetic field, I_{C2} can be changed correspondingly. This in-

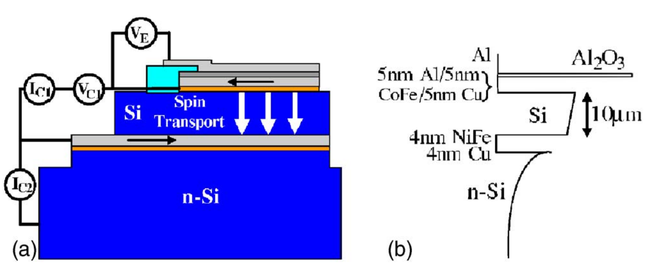

FIG. 1. (Color online) (a) Schematic illustration of the Si spin field-effect device used in this work, and (b) associated conduction band diagram. The vertical structure (top to bottom) is 40 nm Al/Al_2O_3/5 nm Al/5 nm $Co_{84}Fe_{16}$/5 nm Cu/10 μm undoped Si/4 nm $Ni_{80}Fe_{20}$/4 nm Cu/*n*-Si. Hot electrons are injected by an emitter voltage (V_E) from Al ballistically through the $Al/Co_{84}Fe_{16}$/Cu anode base and into the conduction band of the 10 μm thick undoped Si drift layer forming injected current I_{C1}. Detection on the other side is with spin-dependent ballistic hot-electron transport through the $Ni_{80}Fe_{20}$ thin film. Our spin-transport signal is the ballistic current transported into the conduction band of the *n*-Si collector (I_{C2}).

[a)]Electronic mail: bqhuang@udel.edu

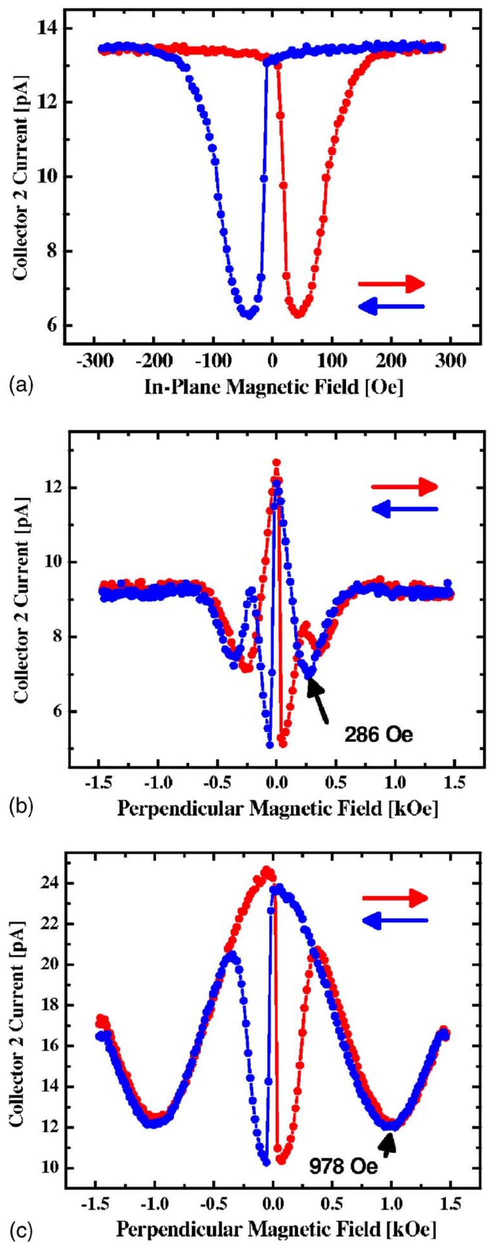

FIG. 2. (Color online) (a) In-plane spin-valve effect for the device with emitter tunnel junction bias $V_E=-1.6$ V and $V_{C1}=0$ V at 85 K, showing $\approx 115\%$ magnetocurrent ratio. (b) Spin precession and dephasing (Hanle effect) in a perpendicular magnetic field with $V_E=-1.6$ V and accelerating voltage $V_{C1}=0$ V. (c) Same as in (b), but with $V_{C1}=3$ V.

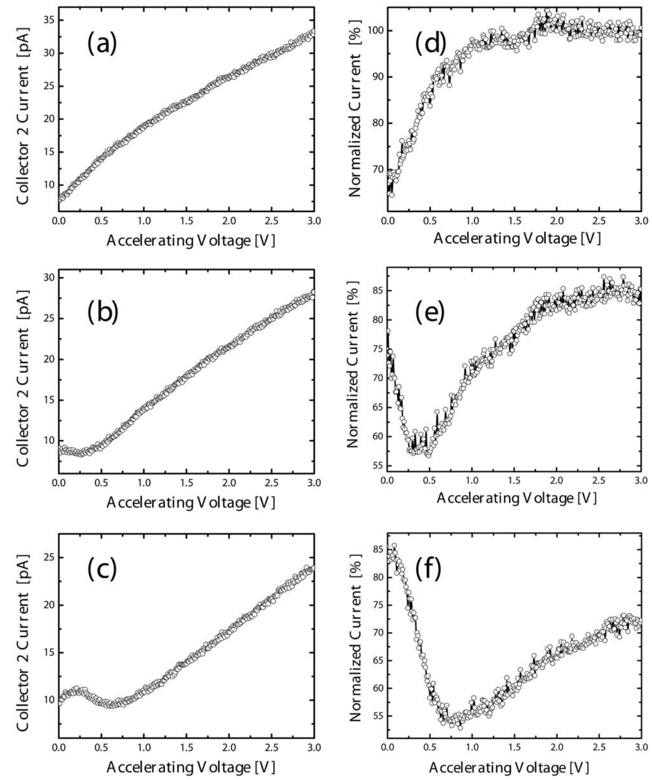

FIG. 3. [(a)–(c)] Spin detection current I_{C2} as a function of accelerating voltage bias V_{C1} in a fixed perpendicular magnetic field. The magnetic field is 191, 380, and 560 Oe for (a)–(c), respectively. (d)–(f) shows (a)–(c), respectively, normalized by I_{C2} spectroscopy in zero magnetic field.

plane spin-valve hysteresis at constant emitter bias $V_E=-1.6$ V is shown in Fig. 2(a). The magnetocurrent ratio $\mathrm{MC}=(I_{C2}^{\mathrm{P}}-I_{C2}^{\mathrm{AP}})/I_{C2}^{\mathrm{AP}}$, where the superscripts P and AP refer to parallel and antiparallel FM injector/detector magnetization configuration, respectively, is approximately 115%, much higher than in the devices we reported before.[14,20] This magnetocurrent ratio, enabled by (i) avoiding silicide formation with the injector FM and (ii) using ballistic spin filtering, corresponds to a conduction electron current spin polarization of at least $\mathcal{P}=(I_{C2}^{\mathrm{P}}-I_{C2}^{\mathrm{AP}})/(I_{C2}^{\mathrm{P}}+I_{C2}^{\mathrm{AP}})=\mathrm{MC}/(\mathrm{MC}+2)\approx 37\%$.

Spin precession measurements of I_{C2} in a perpendicular magnetic field[24,25] at different accelerating voltage biases V_{C1} across the Si spin transport layer were performed, as shown in Figs. 2(b) and 2(c). Due to a small in-plane component of the applied magnetic field, I_{C2} drops when the external perpendicular magnetic field is swept through zero because the $Ni_{80}Fe_{20}$ detector magnetization switches at low coercive field. At approximately 500 Oe, the parallel magnetization configuration is regained when the $Co_{84}Fe_{16}$ switches. The first extrema away from zero applied field (indicated with arrows) correspond to magnetic field conditions such that the precession angle $\theta=\omega\tau=\pi$ (so that final spin direction and analyzing FM magnetization are antiparallel), where τ is the transit time from injector to detector and ω is the precession angular frequency $g\mu_B B/\hbar$. In this expression, g is the electron spin g-factor, μ_B is the Bohr magneton, B is the magnetic field, and $\hbar$ is the reduced Planck constant. Since $\tau\approx L/(\mu E)$, where $L=10$ μm is the transport distance through the undoped Si, μ is the electron mobility, and E is the electric field, the accelerating voltage controls the transit time and hence final spin precession angle through $E=V_{C1}/L$. As shown in Figs. 2(b) and 2(c), with an increase of the accelerating voltage bias across the Si spin transport layer from 0 to 3 V, the magnetic field corresponding to π final spin precession angle increases from 286 to 978 Oe due to the associated reduction of the transit time and the subsequent need for higher precession frequency.

Although Figs. 2(b) and 2(c) show measurements at fixed electric field under conditions of varying magnetic field, we can alternatively change θ at fixed perpendicular magnetic field by varying the electric field. Refer to the partial parallel magnetization curve in the Hanle measurements, which corresponds to the right-left (blue) sweep in positive field shown in Figs. 2(b) and 2(c). From these measurements, it can be seen that if the fixed perpendicular magnetic field is smaller than 286 Oe, an increase of V_{C1} past 0 V causes a continual increase of I_{C2} because the precession angle does not pass through π. For fixed perpendicular magnetic fields slightly larger than 286 Oe, I_{C2} will first decrease with increased V_{C1} as the precession angle approaches π, and then continually increase.

This electric field dependence of I_{C2} at fixed perpendicular magnetic fields, and in a parallel injector/detector magnetization configuration, is shown in Figs. 3(a)–3(c) for 191, 380, and 560 Oe, respectively. Although there is an initial decrease in the measured current at applied fields above 286 Oe as predicted, an ascending trend is dominant due to the increase of injected current (I_{C1}) which drives I_{C2}.[26] This is likely due to enhanced hot-electron collection efficiency under applied bias.[27]

One straightforward solution to this problem is to continue to improve the spin injection efficiency and output current magnitude so that the I_{C2} change due to precession angle control will make the magnetically independent increase negligible. However, we can eliminate this effect artificially by normalizing Figs. 3(a)–3(c) with $I_{C2}(V_{C1})$ in zero magnetic field. The result, shown in Figs. 3(d)–3(f), respectively, agrees very well with our expectation based on the analysis of spin precession measurements [Figs. 2(b) and 2(c)].

In summary, we have presented measurements of a silicon spin transport device showing output current modulation through voltage control of spin precession. Therefore, it comprises operation as a transit-time spinFET. This was enabled by an improved spin-polarized hot-electron injector utilizing ballistic spin filtering. Our work presents dual ways to manipulate the spin direction in spintronic devices: magnetic, through precession frequency ω, and electric, through transit time τ.

This work was supported in part by DARPA/MTO.

1. S. Datta and B. Das, Appl. Phys. Lett. **56**, 665 (1990).
2. I. Žutić, J. Fabian, and S. Das Sarma, Rev. Mod. Phys. **76**, 323 (2004).
3. D. D. Awschalom and M. E. Flatté, Nat. Phys. **3**, 153 (2007).
4. S. Sahoo, T. Kontos, J. Furer, C. Hoffmann, M. Gräber, A. Cottet, and C. Schönenberger, Nat. Phys. **1**, 99 (2005); I. Zutic and M. Fuhrer, *ibid.* **1**, 85 (2005).
5. A. Cottet, T. Kontos, W. Belzig, C. Schönenberger, and C. Bruder, Europhys. Lett. **74**, 320 (2006).
6. A. M. Tyryshkin, S. A. Lyon, A. V. Astashkin, and A. M. Raitsimring, Phys. Rev. B **68**, 193207 (2003).
7. I. Žutić, J. Fabian, and S. C. Erwin, Phys. Rev. Lett. **97**, 026602 (2006).
8. Y. K. Kato, R. C. Myers, A. C. Gossard, and D. D. Awschalom, Science **306**, 1910 (2004).
9. V. Sih, R. C. Myers, Y. K. Kato, W. H. Lau, A. C. Gossard, and D. D. Awschalom, Nat. Phys. **1**, 31 (2005).
10. J. A. Gupta, R. Knobel, N. Samarth, and D. D. Awschalom, Science **292**, 2458 (2001).
11. X. Lou, C. Adelmann, M. Furis, S. A. Crooker, C. J. Palmstrom, and P. A. Crowell, Phys. Rev. Lett. **96**, 176603 (2006).
12. X. Lou, C. Adelmann, S. A. Crooker, E. S. Garlid, J. Zhang, S. M. Reddy, S. D. Flexner, C. J. Palmstrom, and P. A. Crowell, Nat. Phys. **3**, 197 (2007).
13. M. Holub, J. Shin, D. Saha, and P. Bhattacharya, Phys. Rev. Lett. **98**, 146603 (2007).
14. I. Appelbaum, B. Huang, and D. Monsma, Nature (London) **447**, 295 (2007).
15. I. Appelbaum and D. Monsma, Appl. Phys. Lett. **90**, 262501 (2007).
16. J. Y. Veuillen, J. Derrien, P. A. Badoz, E. Rosencher, and C. Danterroches, Appl. Phys. Lett. **51**, 1448 (1987).
17. J. S. Tsay and Y. D. Yao, Appl. Phys. Lett. **74**, 1311 (1999).
18. J. S. Tsay, C. S. Yang, Y. Liou, and Y. D. Yao, J. Appl. Phys. **85**, 4967 (1999).
19. I. Žutić and J. Fabian, Nature (London) **447**, 269 (2007).
20. B. Huang, L. Zhao, D. Monsma, and I. Appelbaum, Appl. Phys. Lett. **91**, 052501 (2007).
21. D. J. Monsma, J. C. Lodder, Th. J. A. Popma, and B. Dieny, Phys. Rev. Lett. **74**, 5260 (1995).
22. D. J. Monsma, R. Vlutters, and J. C. Lodder, Science **281**, 407 (1998).
23. R. Jansen, J. Phys. D **36**, R289 (2003).
24. M. Johnson and R. H. Silsbee, Phys. Rev. B **37**, 5326 (1988).
25. M. Johnson and R. H. Silsbee, Phys. Rev. Lett. **55**, 1790 (1985).
26. B. Huang, D. Monsma, and I. Appelbaum, J. Appl. Phys. **102**, 013901 (2007).
27. C. Crowell and S. Sze, in *Physics of Thin Films*, edited by G. Hass and R. Thun (Academic, New York, 1967), Vol. 4, p. 325.